CCS Chemistry

RESEARCH ARTICLE

Received: Feb. 19, 2025 | Accepted: Mar. 20, 2025 | Published: May 10, 2025

Copper Nanoparticles Stabilized by Adjacent Methyl Groups on Silica for Durable Catalysts

Lujie Liu[1†], Jiaye Lu[2†], Mingjie Liu[1], Hong Wang[3], Jinyang Zhang[3], Guangxian Xu[3], Zhandong Wang[3], Yang Liu[4], Jie Liang[4], Xinhua Gao[4], Yating Lv[1], Yida Zhou[5], Shutao Xu[5], Lina Li[6]*, Xiao-Ming Cao[2,7]* & Liang Wang[1]*

[1]Key Laboratory of Biomass Chemical Engineering of the Ministry of Education, College of Chemical and Biological Engineering, Zhejiang University, Hangzhou 310027, [2]Joint International Research Laboratory of Precision Chemistry and Molecular Engineering, Feringa Nobel Prize Scientist Joint Research Center, School of Chemistry and Molecular Engineering, East China University of Science and Technology, Shanghai 200237, [3]National Synchrotron Radiation Laboratory, University of Science and Technology of China, Hefei, Anhui 230029, [4]State Key Laboratory of High-efficiency Utilization of Coal and Green Chemical Engineering, School of Chemistry and Chemical Engineering, Ningxia University, Yinchuan 750021, [5]National Engineering Research Center of Lower-Carbon Catalysis Technology, Dalian Institute of Chemical Physics, Chinese Academy of Sciences, Dalian 116023, [6]Shanghai Synchrotron Radiation Facility, Shanghai Advanced Research Institute, Chinese Academy of Sciences, Shanghai 201204, [7]State Key Laboratory of Synergistic Chem-Bio Synthesis, School of Chemistry and Chemical Engineering, Shanghai JiaoTong University, Shanghai 200240

**Corresponding authors: lilina@sinap.ac.cn; xmcao@sjtu.edu.cn; liangwang@zju.edu.cn; †L. Liu and J. Lu contributed equally to this work.*

Cite this: *CCS Chem.* **2025**, Just Published. DOI: 10.31635/ccschem.025.202505638

Stabilizing metal nanoparticle catalysts typically requires supports with strong interactions, yet this poses a significant challenge for relatively inert supports (e.g., silica). In this study, we address this issue by strategically introducing methyl groups adjacent to copper nanoparticles on the silica surface. These methyl groups do not directly interact with the copper nanoparticles but effectively stabilize them against sintering during catalytic reactions. This is due to the significantly elevated energy barrier for copper nanoparticles to migrate through the noninteracting methyl groups, thereby preventing the sintering via migration-coalescence or Ostwald ripening routes. Consequently, this strategy leads to exceptional durability of silica-supported copper catalysts in the hydrogenation of dimethyl oxalate, a reaction that suffers from deactivation from copper sintering, and outperforms generally supported copper nanoparticle catalysts.

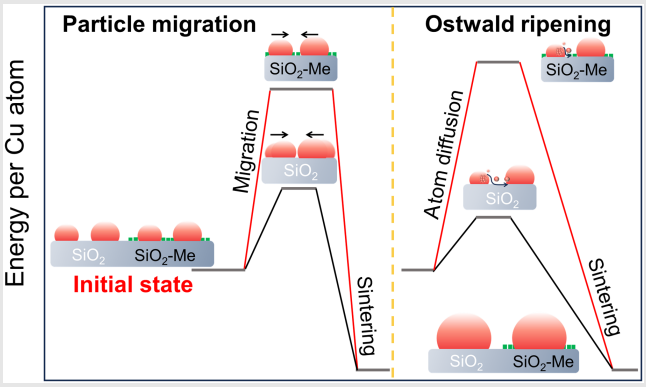

Keywords: metal sintering, copper catalyst, silica support, methyl groups, ethylene glycol synthesis

Citation: *CCS Chem.* **2025**, Just Published. DOI: 10.31635/ccschem.025.202505638
Link to VoR: https://doi.org/10.31635/ccschem.025.202505638

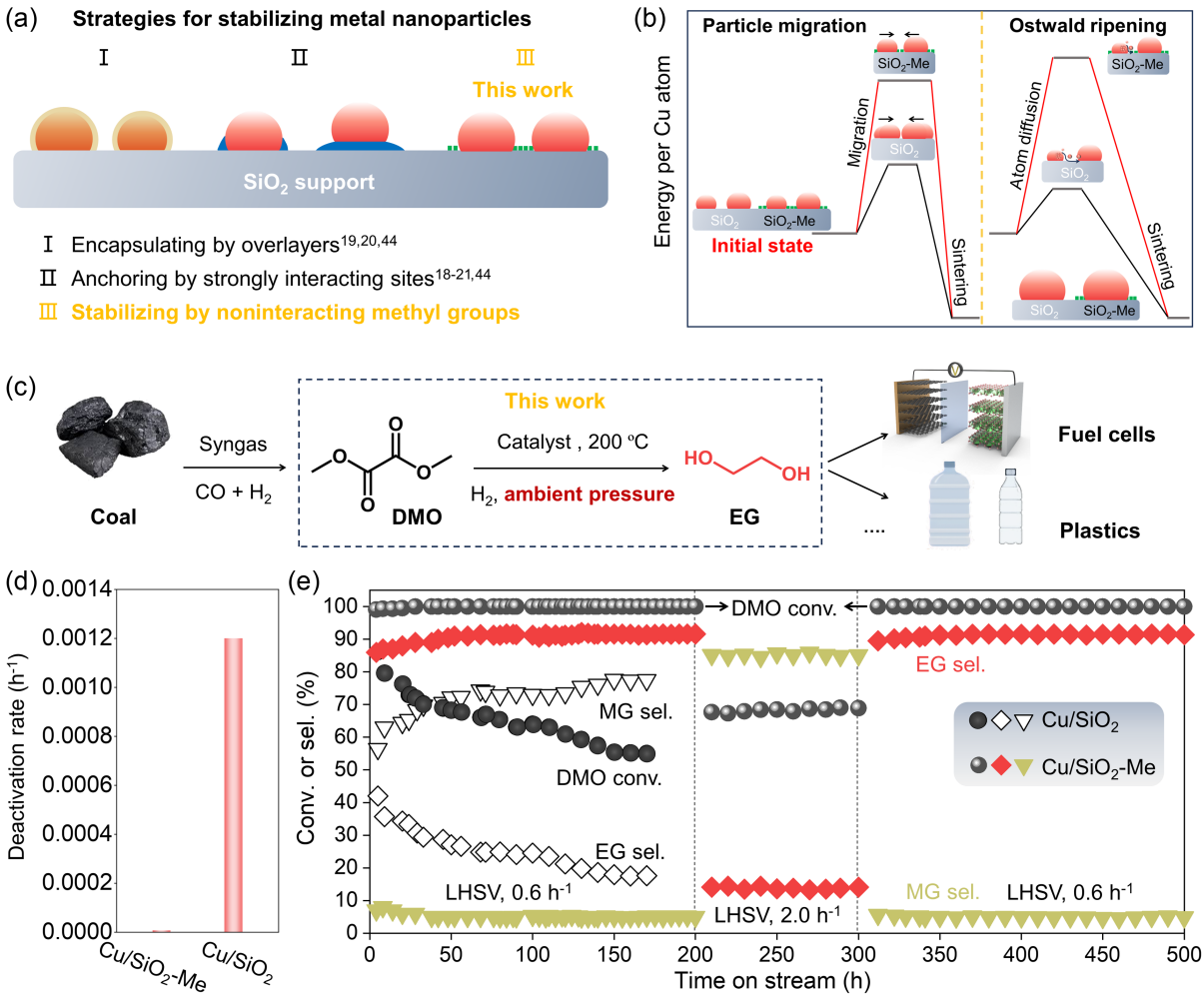

Figure 1 | *Design and achieved results of sintering-resistant copper catalyst. (a) Different strategies for stabilizing metal nanoparticles against sintering. (b) Schematic representation of the differences in the energetics for the sintering of Cu nanoparticles on the silica surface with and without methyl groups. The migrating state with Cu nanoparticles or atomic Cu intermediates on methyl groups has extremely high free energy that is difficult to move. (c) Scheme showing the synthetic pathways of EG and its applications. (d) The deactivation rates of these two catalysts in DMO hydrogenation. (e) Data showing the durability of silica-supported Cu catalysts with and without methyl groups in DMO hydrogenation at 200 °C and 0.1 MPa. The error bounds for conversion and selectivity were ±2%.*

Introduction

The supported metal nanoparticle catalysts have been industrially used in a wide range of reactions, but the nanoparticles tend to grow into larger ones during the catalysis.[1–5] This leads to a decrease in metallic specific surface area or the number of interfacial sites, which results in irreversible deactivation.[4,5] In the practical reaction processes, shutting down the industrial plant and replacing the spent catalysts with new ones becomes necessary and leads to high costs.[6] Rational design of catalyst structures that could efficiently prevent metal nanoparticle sintering is of great importance.

Metal nanoparticle sintering usually proceeds along routes including the formation and diffusion of atomic metal intermediates (Ostwald ripening) and/or nanoparticle migration and coalescence on the solid support.[7–11] To overcome these issues, the general strategy has been to encapsulate the nanoparticles with oxide/carbon overlayers or in the nanopores,[12–14] which efficiently prevent nanoparticle migration and/or metal detaching as movable atomic intermediates, thus enhancing the stability (Figure 1a, I). However, these overlayers block the metal nanoparticle surface to reduce the number of active sites, leading to a partial loss of catalytic activity.[14] Another route for metal stabilization is optimizing the metal-support interactions,[15–20] which simultaneously stabilize the metal nanoparticles and maintain the number of accessible surfaces. Following this route, the reducible oxides (e.g., CeO_2, TiO_2) have been extensively used to

Citation: *CCS Chem.* **2025**, Just Published. DOI: 10.31635/ccschem.025.202505638
Link to VoR: https://doi.org/10.31635/ccschem.025.202505638

obtain stable metal nanoparticle catalysts, due to their strong interaction with the metal nanoparticles.[19]

A more recent design employs the hybrid supports involving components with distinguishable interactions with the metal species, which further improves the sintering resistance.[20–23] In this design, the ceria islands on silica efficiently stabilize the Pt single atoms (Figure 1a, II);[21] physically mixing ceria with Cu/SiO_2[22] or Pt/Al_2O_3[23] catalyst that promotes the metal migration from silica or alumina to ceria for stabilization. In these cases, the metal species tend to stabilize in the strong interaction region because of the large adhesion energy of metal nanoparticles to the reducible oxide surface,[24] and such bonding usually changes the intrinsic catalytic properties of the original metal nanoparticles. In contrast, for metal nanoparticles on relatively inert supports, such as amorphous silica, which is a typical support with wide industrial applications,[25–27] their stabilization remains a great challenge.[28]

Herein, we achieve stabilization of metal nanoparticles on relatively inert support by introducing methyl groups adjacent to copper nanoparticles on the silica surface (Figure 1a, III). These methyl groups are chemically inert and noninteracting with copper, thus avoiding problems caused by classical methods, including blocking the metal surface or changing the intrinsic catalytic properties. Instead, the methyl groups establish a significantly elevated energy barrier for copper migrating through them, forming a steric effect that effectively switches off the migration-coalescence and Ostwald ripening sintering mechanisms (Figure 1b). The hydrogenation of dimethyl oxalate (DMO) is an important reaction in the coal-to-ethylene glycol industrial process but suffers from catalyst deactivation from Cu sintering (Figure 1c,d).[29–32] The silica supported catalyst with methyl groups shows superior durability with an extremely low deactivation rate (based on ethylene glycol (EG) yield, Figure 1d). The deactivation is negligible, even under harsh reaction conditions. In contrast, the catalyst without methyl groups shows a high deactivation rate under the equivalent test.

Experimental Methods

The silica-supported Cu catalysts were synthesized by the method we reported previously.[28] 2.28 g of Cu $(NO_3)_2 \cdot 3H_2O$ was dissolved in aqueous ammonia solution (7.5 g of $NH_3 \cdot H_2O$ diluted with 120 mL of deionized water). After stirring for 10 min, 1.40 g of SiO_2 was added to the solution and stirred vigorously at 80 °C for another 6 h. Then, the sample was filtrated, dried at 100 °C overnight, and calcined at 350 °C for 3 h with a heating rate of 1 °C/min. The obtained catalyst was prereduced with hydrogen at 300 °C for 2 h before the catalytic test. In synthesizing the methyl-modified silica (SiO_2-Me) supported Cu catalysts, similar procedures were carried out unless 1.0 g of tetrahydrofuran was added into the mixture to promote the dispersion of support and deposition of Cu species onto the support. The samples were treated by calcination and prereduction under the same conditions as that for the Cu/SiO_2. More details for materials, catalyst preparation, characterization, catalytic tests, and computational methods can be found in the Supporting Information.

Results and Discussion

Synthesis, catalysis, and characterization

The silica modified by methyl groups was prepared through the cohydrolysis of diethoxydimethylsilane (DEMS) and tetraethyl orthosilicate (TEOS). Then Cu nanoparticles were loaded following the ammonia-assisted method, obtaining the Cu/SiO_2-Me sample with a Cu content of 30 wt % and methyl content of 10 mol % (molar ratio of $n_{(DEMS)}$ to $n_{(DEMS)}+n_{(TEOS)}$ in the starting mixture at 1/10). The presence of methyl groups was confirmed by Fourier transform infrared (FT-IR) spectra, the water droplet contact angle, and nuclear magnetic resonance (NMR) characterizations (Supporting Information Figures S1–S3 and Table S1). In contrast, the reference Cu/SiO_2 catalyst was synthesized by directly loading Cu on amorphous silica, obtained from the hydrolysis of TEOS without DEMS, with a content of 30 wt %.

The catalytic performance of fresh Cu/SiO_2 and Cu/SiO_2-Me were initially studied in DMO hydrogenation at ambient pressure with a liquid hourly space velocity (LHSV) of 0.6 h^{-1} (mL_{DMO} mL_{cat}^{-1} h^{-1}) based on a feeding rate of DMO per milliliter of catalyst at 200 °C (Figure 1e). In the continuous reaction, the DMO conversion over Cu/SiO_2 catalyst was continuously decreased, giving 55.5% after reaction for 150 h (Figure 1e). The EG selectivity was downhill during the process, with methyl glycolate (MG, a semihydrogenation product) becoming a major product. The deactivation for Cu/SiO_2 was due to the sintering of Cu nanoparticles, where the spent catalyst showed the average Cu nanoparticle size of 9.9 ± 5.7 nm (Supporting Information Figure S4), versus 5.4 ± 1.5 nm on the fresh sample. This result is in good agreement with the general phenomenon of Cu sintering in DMO hydrogenation, particularly under ambient pressure.[29] In contrast, the full conversion of DMO and EG selectivity up to 91.5% were maintained over the Cu/SiO_2-Me catalyst during the test for 200 h. To evaluate the Cu/SiO_2-Me catalyst with incomplete conversion of DMO, we increased the LHSV to 2.0 h^{-1}, and the Cu/SiO_2-Me exhibited constant performance in another 100 h with DMO conversion of ~68% and MG selectivity of ~85%. After switching the LHSV back to 0.6 h^{-1}, the Cu/SiO_2-Me catalyst showed similar catalytic performance to that in the initial reaction for the continuous test in another 200 h. Given the fact that any activity decrease of Cu catalyst would sensitively reduce the EG selectivity and enhance the MG selectivity, the

Citation: *CCS Chem.* **2025**, Just Published. DOI: 10.31635/ccschem.025.202505638
Link to VoR: https://doi.org/10.31635/ccschem.025.202505638

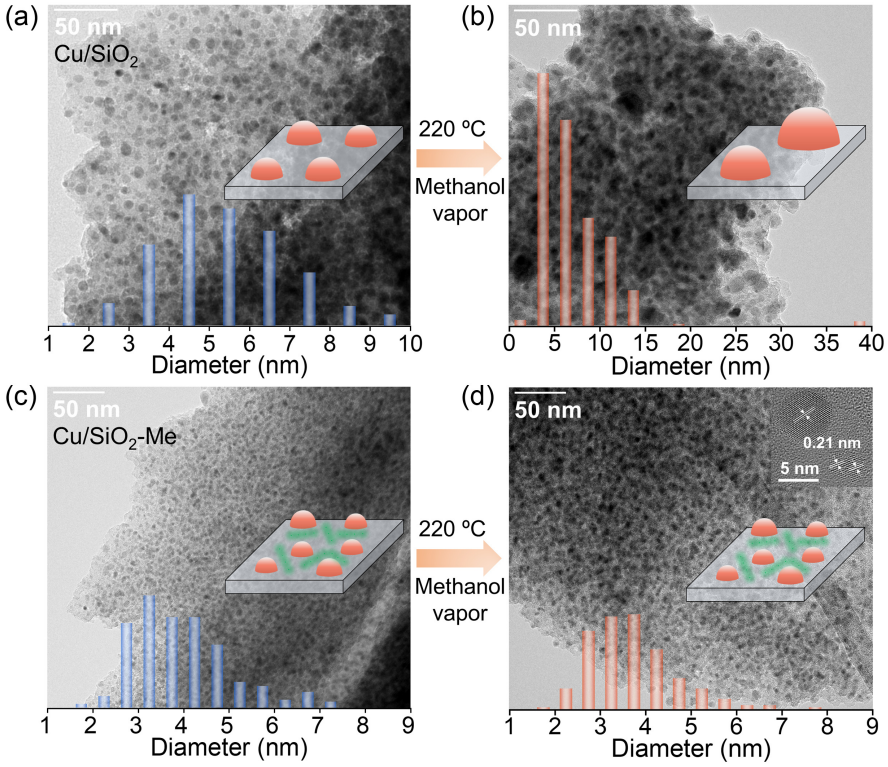

Figure 2 | *TEM images of (a, b) Cu/SiO_2 and (c, d) Cu/SiO_2-Me before and after the methanol treatment at 220 °C for 96 h. Inset in a–d, Cu nanoparticle size distributions of the fresh and methanol-treated catalysts; inset in d, high-resolution TEM image of the methanol-treated catalyst, where 0.21 nm corresponds to the (111) plane of Cu.*[36]

constant DMO conversion and EG/MG selectivity in the test for 500 h sufficiently supported the durability of Cu/SiO_2-Me catalyst. Transmission electron microscopy (TEM) images of the spent Cu/SiO_2-Me catalyst after the test for 500 h showed the small-size Cu nanoparticles with an average size of 4.0 ± 1.0 nm (Supporting Information Figure S5), similar to the fresh catalyst.

The fresh Cu/SiO_2 and Cu/SiO_2-Me samples had Cu nanoparticles with average sizes at 5.4 ± 1.5 and 3.7 ± 1.0 nm, respectively, as observed in the TEM images (Figure 2a,c). We evaluated the stability of these Cu nanoparticles by treating them in methanol vapor, a condition that usually causes Cu sintering.[28,29,33–35] After the methanol treatment at 220 °C for 96 h (methanol feeding rate of 0.03 mL_{liquid}/min in hydrogen with flow rate at 25 mL/min), many Cu nanoparticles on the Cu/SiO_2 were sintered into large particles with an average size of 6.7 ± 3.4 nm (Figure 2b and Supporting Information Figure S6), and some nanoparticles were even larger than 35 nm (Supporting Information Figure S6). In contrast, the Cu/SiO_2-Me maintained the Cu nanoparticles, giving an average size of 3.9 ± 1.1 nm (Figure 2d and Supporting Information Figure S7) after the equivalent treatment, which is similar to the fresh Cu/SiO_2-Me sample (3.7 ± 1.0 nm, Figure 2c). These data suggest that introducing methyl groups onto the SiO_2 surface significantly suppressed the Cu nanoparticle sintering in methanol vapor.

To gain insights into the surface electronic state of Cu species, the Cu/SiO_2 and Cu/SiO_2-Me samples before and after methanol treatment at 220 °C were characterized by X-ray photoelectron spectroscopy (Supporting Information Figure S8) with Cu LMM Auger electron spectroscopy. A broad and asymmetrical peak was obtained in these samples (Supporting Information Figure S9), and it was deconvoluted into two peaks at 916.1 (Cu^0) and 913.1 eV (Cu^+).[37] The ratios of $Cu^+/(Cu^0+Cu^+)$ were about 45% and 56% for the fresh Cu/SiO_2 and Cu/SiO_2-Me samples, respectively. After methanol vapor treatment at 220 °C for 96 h, the Cu^+ species on the Cu/SiO_2 were reduced into a metallic state, giving the $Cu^+/(Cu^0+Cu^+)$ ratio of 35% over the Cu/SiO_2. This was due to the Cu sintering into large particles, which resulted in the weak interaction between metallic Cu and silica support since the Cu^+ species originated from the $Cu^{\delta+}$-O-SiO_x interface.[28,29,38–42] In contrast, the Cu^0 and Cu^+ signals were unchanged on the Cu/SiO_2-Me before and after methanol vapor treatment, giving a similar $Cu^+/(Cu^0+Cu^+)$ ratio at 55% (Supporting Information Figure S9). This can be ascribed to the sintering resistance of Cu nanoparticles on the Cu/SiO_2-Me, where the $Cu^{\delta+}$-O-SiO_x interface was well maintained during the treatment. This

Citation: *CCS Chem.* **2025**, Just Published. DOI: 10.31635/ccschem.025.202505638
Link to VoR: https://doi.org/10.31635/ccschem.025.202505638

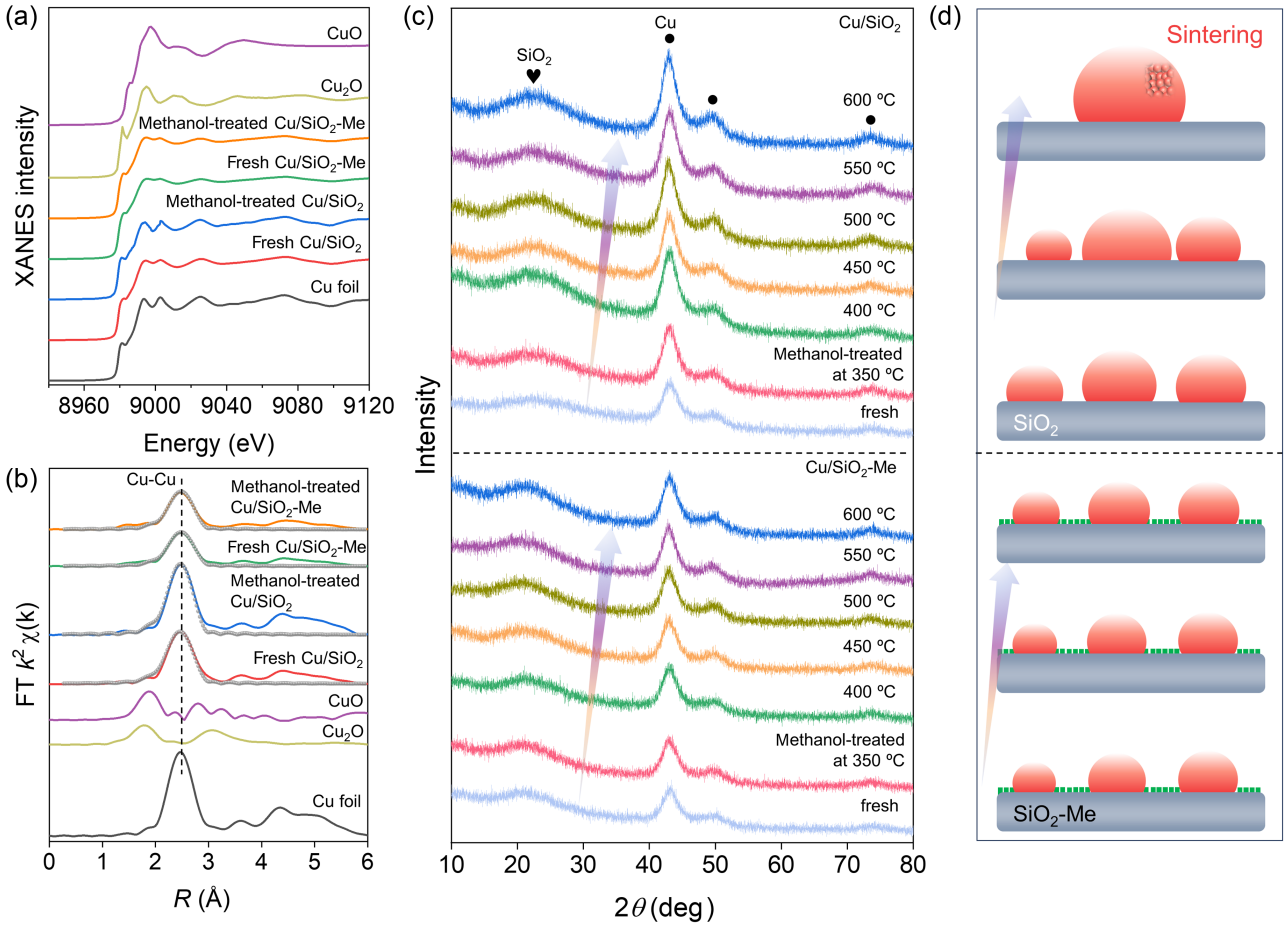

Figure 3 | *(a) Normalized Cu K-edge XANES spectra and (b) Fourier transformed magnitudes of the experimental Cu K-edge EXAFS of fresh and methanol-treated Cu/SiO_2 and Cu/SiO_2-Me catalysts. (c) In situ XRD patterns characterizing the change of Cu nanoparticles on the Cu/SiO_2 and Cu/SiO_2-Me during the methanol treatment from 350 to 600 °C. (d) Scheme showing sintering of Cu on the SiO_2 and sintering-resistant of Cu on the SiO_2-Me.*

result was further supported by the CO-adsorption FT-IR spectra (Supporting Information Figure S10).

The Cu/SiO_2 and Cu/SiO_2-Me catalysts before and after the methanol treatment at 220 °C were characterized by X-ray adsorption fine structures spectroscopy. The X-ray absorption near-edge structure (XANES) spectrum of the fresh Cu/SiO_2 was close to the reference sample of Cu foil, suggesting that Cu^0 species were dominant with some oxidation-state Cu (Figure 3a). After the methanol treatment, the average valence of Cu species on the Cu/SiO_2 was further reduced to Cu^0 since the spectrum fell more closely to the Cu foil. This can be reasonably ascribed to the sintering of Cu during the methanol treatment. The extended X-ray adsorption fine structure (EXAFS) fitting analysis (Figure 3b) showed the increased coordination number (CN) of the Cu–Cu shell from 8.3 to 9.6 (Supporting Information Table S2) for the methanol-treated Cu/SiO_2 catalyst. In contrast, the XANES spectra were unchanged for the Cu/SiO_2-Me regardless of methanol treatment (Figure 3a), and the CN of Cu–Cu shell was 4.8 and 4.9 (Supporting Information Table S2) for the fresh and methanol-treated Cu/SiO_2-Me catalysts, respectively. The results above confirm that Cu nanoparticle size and oxidization state were stable in methanol vapor on the support of methyl-modified silica.

Figure 3c shows the in situ X-ray diffraction (XRD) characterizing the change of Cu nanoparticles in methanol vapor. A temperature-programmed condition ranging from 350 to 600 °C was used in this study to accelerate the Cu sintering that benefitted the test. Compared with SiO_2 support, the fresh Cu/SiO_2 showed additional peaks at 43.3°, 50.1°, and 73.4°, attributed to the diffraction of metallic Cu. After methanol vapor treatment at 350 °C, the peaks assigned to Cu^0 species became more intense on the Cu/SiO_2. Further increasing the temperature led to the continuously enhanced intensities of these peaks because of the sintering of Cu nanoparticles (Figure 3d). In contrast, these diffractions on the Cu/SiO_2-Me were unchanged during the methanol treatment at 350 and 400 °C, suggesting high

Citation: *CCS Chem.* **2025**, Just Published. DOI: 10.31635/ccschem.025.202505638
Link to VoR: https://doi.org/10.31635/ccschem.025.202505638

stability. After treatment at 450–600 °C, the diffractions of Cu were slightly enhanced, which could be due to the Cu sintering under such harsh conditions. Even after treatment at 600 °C, an extremely harsh condition for Cu, the diffraction of metallic Cu on the Cu/SiO_2-Me was still much weaker than that on the Cu/SiO_2.

The aforementioned results confirm the significantly enhanced stability of Cu nanoparticles on the silica support containing methyl groups. Notably, this feature is not relative to the extensively studied encapsulated structure because the Cu nanoparticles were loaded on the readily prepared SiO_2-Me support, rather than a post modification of the Cu/SiO_2 catalyst, while the latter usually leads to blocking the metal surface.[19,43,44] In addition, the N_2 sorption isotherms gave a Brunauer–Emmett–Teller (BET) surface area (S_{BET}) of 186 m^2/g for the Cu/SiO_2, while it was 486 m^2/g for the Cu/SiO_2-Me due to the cohydrolysis synthesis containing organic groups (Supporting Information Figure S11).

One might ascribe the fact that the larger surface area of SiO_2-Me support contributed to the sintering resistance of Cu nanoparticles rather than the methyl groups. To exclude this hypothesis, we removed the methyl groups on the SiO_2-Me by ozone treatment at room temperature and maintained the high surface area. Then the Cu nanoparticles were loaded to obtain a Cu/SiO_2-Me-O_3 sample (Supporting Information Figures S12 and S13). This sample had a surface area of 553 m^2/g, which was higher than that of the Cu/SiO_2-Me because of the removal of organic groups (Supporting Information Figures S14 and S15). The Cu nanoparticle size on the fresh Cu/SiO_2-Me-O_3 catalyst was 7.6 ± 3.8 nm, larger than that on the methyl-modification silica. Then, the Cu particles were sintered into 9.7 ± 4.5 nm after a menthol vapor treatment (Supporting Information Figure S16). All these data confirm the crucial role of methyl groups in stabilizing the Cu nanoparticles against sintering.

We also studied the stability of organic groups on the catalyst. Compared with the thermogravimetric differential thermal analysis of Cu/SiO_2, the Cu/SiO_2-Me showed exothermic additional signals at 560 and 620 °C (Supporting Information Figure S17), due to the combustion of methyl groups,[45,46] and these features benefitted the catalysis. The water-droplet contact angle and NMR characterizations (Supporting Information Figures S18 and S19) of the spent Cu/SiO_2-Me catalyst still showed obvious signals assigned to the methyl groups, which were similar to those of the fresh catalyst, confirming the stability of methyl groups under the DMO hydrogenation conditions.

Catalysis at ambient pressure

The catalytic performances of Cu/SiO_2 and Cu/SiO_2-Me were compared at ambient pressure with an LHSV of 0.6 h^{-1} (Figure 4a). The Cu/SiO_2 showed an initial DMO conversion of 86.1% with selectivities to EG and MG of 42.0% and 56.4%, respectively. In contrast, the Cu/SiO_2-Me showed the full conversion of DMO under the equivalent test conditions, with the EG and MG selectivities of 91.5% and 2.5%, respectively. The higher activity of Cu/SiO_2-Me than Cu/SiO_2 should reasonably be attributed to the smaller Cu nanoparticles with more $Cu^{\delta+}$-O-SiO_x interfacial sites that have been identified as crucial for the DMO hydrogenation.[28,29,39,40,42]

Next, the catalytic performances of methanol-treated catalysts were further investigated. Even after harsh treatment in methanol at 220 °C for 96 h, the Cu/SiO_2-Me still showed constant performance in DMO hydrogenation with LHSV between 0.6 and 2.0 h^{-1}, and EG yield was similar to the fresh catalyst (Figure 4b). Under the optimized reaction conditions, the highest EG yield was 91.5% for DMO hydrogenation at ambient pressure (Supporting Information Figure S20).

To optimize the catalytic performance, a series of Cu/SiO_2-Me catalysts with different contents of methyl group (molar ratio of $n_{(DEMS)}$ to $n_{(DEMS)}+n_{(TEOS)}$ in the starting mixtures at 5–25%) were synthesized (Supporting Information Figures S21 and S22). TEM characterization showed average Cu nanoparticle sizes of 4.2–5.4 nm for the fresh samples (Supporting Information Figure S23) with similar reducibility as determined by the temperature-programmed reduction test (Supporting Information Figure S24). In the DMO hydrogenation, the EG yield was increased over catalysts with contents of methyl groups of 5%–10% due to the smaller-size Cu nanoparticles (3.7–4.2 nm vs 5.4 nm of fresh Cu/SiO_2), which reached their highest value of 91.5% over the Cu/SiO_2-Me with methyl group content of 10% (standard catalyst at Cu average size of 3.7 nm, Figure 4c). Further increasing the methyl group content to 25% drastically decreased the EG yield. TEM images showed that the spent catalysts had similar Cu nanoparticle sizes to the fresh catalysts (Supporting Information Figure S25). These data confirm that the methyl groups, regardless of their contents on the catalyst, efficiently stabilized the Cu nanoparticles.

To examine the generality of such modulation, we synthesized the silica-supported catalysts modified with propyl and phenyl groups instead of methyl groups, obtaining the Cu/SiO_2-C_3 and Cu/SiO_2-C_6 catalysts (Supporting Information Figure S26). We evaluated the fresh and methanol-treated (220 °C and 96 h) catalysts in the DMO hydrogenation. As shown in Figure 4d, both catalysts exhibited similar performances regardless of methanol treatment, whereas EG yields were about 77% and 60% over the Cu/SiO_2-C_3 and Cu/SiO_2-C_6, respectively. XRD patterns and TEM analyses also suggested negligible Cu sintering over these catalysts during methanol treatment and catalytic tests in DMO hydrogenation under ambient pressure (Supporting Information Figures S27 and S28). This result demonstrates

Citation: *CCS Chem.* **2025**, Just Published. DOI: 10.31635/ccschem.025.202505638
Link to VoR: https://doi.org/10.31635/ccschem.025.202505638

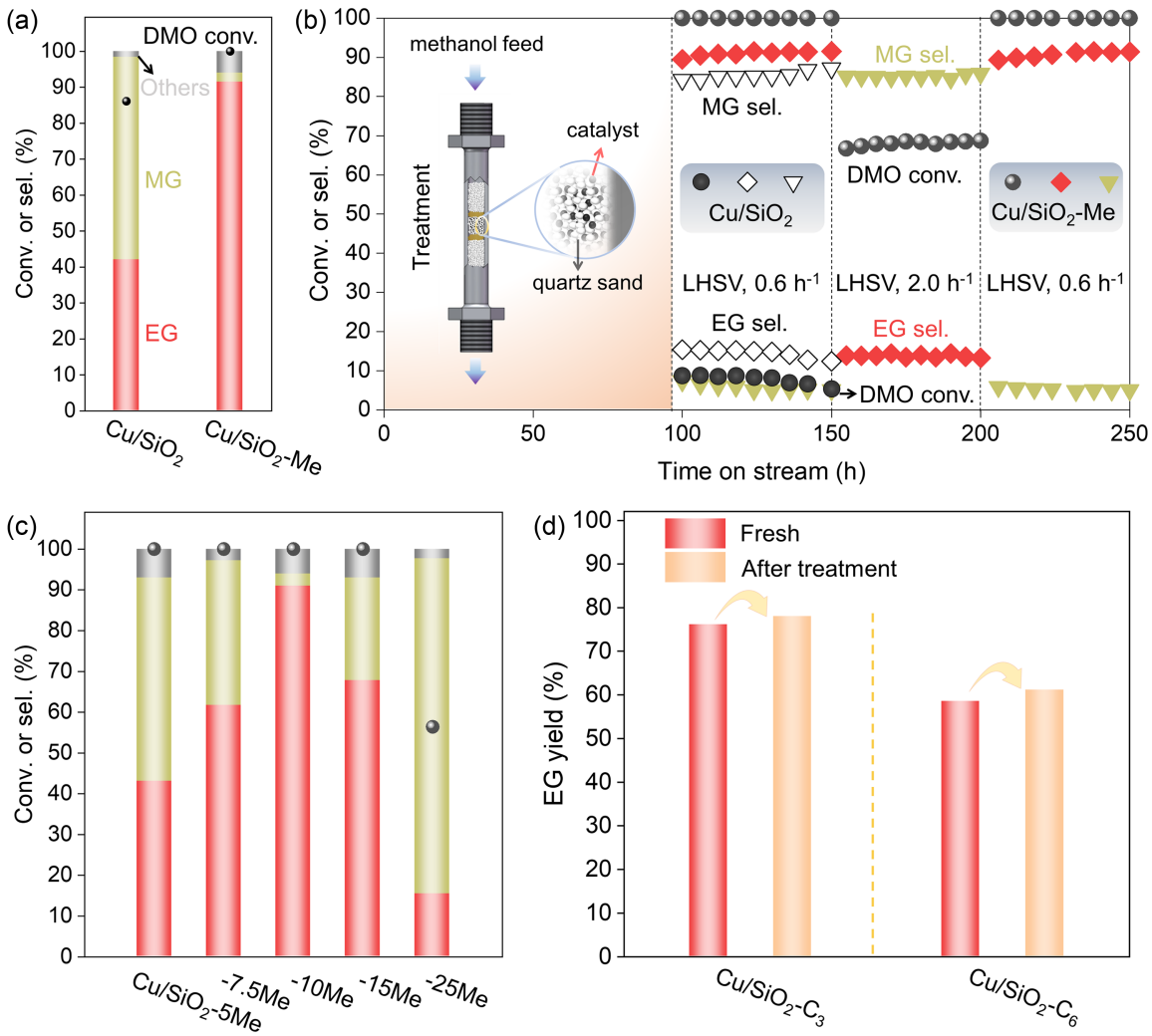

Figure 4 | *(a) Catalytic performances of the Cu/SiO_2 and Cu/SiO_2-10Me in DMO hydrogenation. Reaction conditions: 200 °C, 0.1 MPa, LHSV of 0.6 h^{-1}, n(H_2)/n(DMO) of 160, 100 h. (b) Data showing the effect of methanol treatment (initial 96 h) on the performances of the Cu/SiO_2 and Cu/SiO_2-Me catalysts in DMO hydrogenation. Conditions for methanol treatment: methanol feeding rate of 0.03 mL_{liquid}/min, 220 °C, 96 h. (c) Effect of Me contents on the performances of Cu/SiO_2. (d) Data showing the EG yields in DMO hydrogenation over fresh and methanol-treated Cu/SiO_2-C_3 and modified Cu/SiO_2-C_6 catalysts. The error bounds of conversion and selectivity were ±2%.*

the enhanced stability of Cu nanoparticles on the SiO_2 support when modified with alkyl groups.

Mechanism study

In the preparation of Cu/SiO_2-Me, the Cu nanoparticles were initially loaded on the methyl-modified support. Another strategy was to directly modify the Cu/SiO_2 catalyst through the hydrolysis of DEMS (Cu/SiO_2-Me-P), which enhanced the stability of Cu nanoparticles in DMO hydrogenation.[47] However, such Cu/SiO_2-Me-P catalyst showed lower activity than the Cu/SiO_2 catalyst (Supporting Information Figure S29), due to the partially blocked Cu surface by this method. In addition, we also evaluated the performances of Cu/SiO_2-Me-O_3 catalyst in DMO hydrogenation, giving continuously decreased conversion with reaction time (Supporting Information Figure S30) due to the Cu nanoparticle sintering (Supporting Information Figure S31). These results confirm the pivotal role of methyl groups in achieving a durable catalyst.

Previous research has demonstrated that Cu nanoparticles on silica undergo sintering through particle migration and coalescence under thermal conditions, whereas under chemical triggering conditions, they tend to proceed via Ostwald ripening.[15,33,48] In Ostwald ripening, Cu_1-related intermediates are formed and migrate from small nanoparticles to larger ones to cause sintering. In the migration and coalescence process, metal nanoparticles move toward each other and aggregate to form larger

Citation: *CCS Chem.* **2025**, Just Published. DOI: 10.31635/ccschem.025.202505638
Link to VoR: https://doi.org/10.31635/ccschem.025.202505638

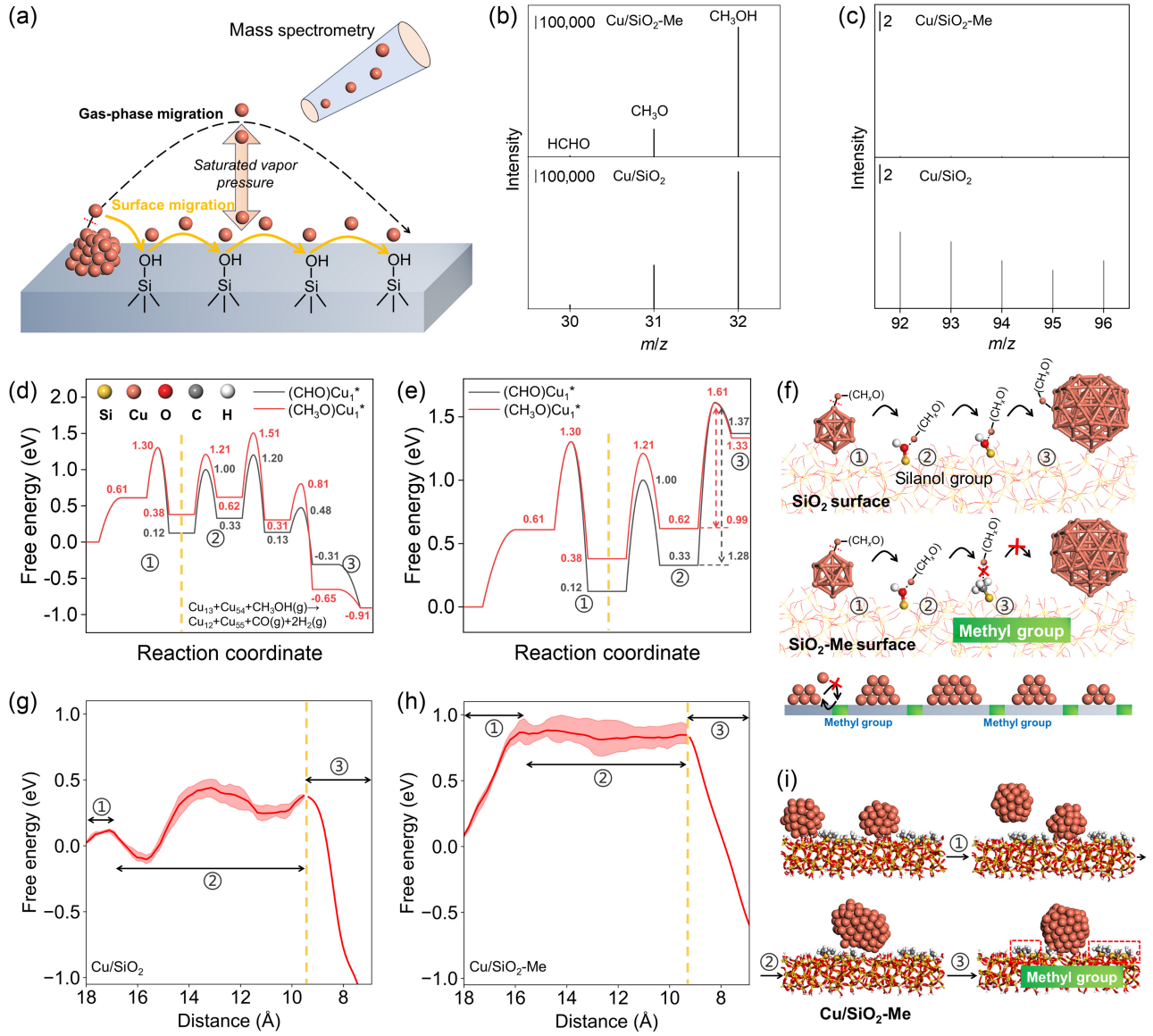

Figure 5 | *(a) Scheme showing the migration of Cu intermediates on the solid surface, and their diffusion into gas phase through a process controlled by saturated vapor pressure, thus benefiting the detection of by SVUV-PIMS. (b, c) Data showing the signals at different m/z regions in the SVUV-PIMS tests characterizing methanol treatment to the Cu/SiO_2 and Cu/SiO_2-Me. The background signals were excluded. (d, e) Free energy diagram for the formation of (CHO)Cu_1* and (CH_3O)Cu_1* intermediates, and their migration (d) from Cu_{13} cluster onto Cu_{55} cluster or (e) from Cu_{13} cluster to Si-CH_3 site. (f) Scheme showing the migration of atomic Cu species on the SiO_2 and SiO_2-Me. (g, h) Free energies of Cu nanoparticle migration onto the neighboring nanoparticle on the SiO_2 and SiO_2-Me, and the reddish area shows the error of the averaged Jarzynski equality curve vs the SMD simulation. (i) Scheme showing the Cu sintering through nanoparticle migration and coalescence on the SiO_2-Me.*

particles. Therefore, the influence of methyl groups on the silica surface in the migration of Cu_1 intermediates and Cu nanoparticles was considered.

In the Ostwald ripening pathway, Cu_1 intermediates typically migrate on the solid surface, while the saturated vapor pressure of the intermediates leads to their partial diffusion into the gas phase (Figure 5a). During DMO hydrogenation, the surface migration should be predominant due to the low saturated vapor pressure of the Cu_1 intermediates at mild temperatures. Nevertheless, it still enabled us to capture the intermediates from the gas phase close to the catalyst surface and identify them using synchrotron vacuum ultraviolet photoionization mass spectrometry (SVUV-PIMS), a highly sensitive technique adept at trace detection.

Our previous study showed that the methanol-triggered Cu surface activation and Cu–Cu cleavage benefitted the formation of Cu_1-related intermediates.[28]

Citation: *CCS Chem.* **2025**, Just Published. DOI: 10.31635/ccschem.025.202505638
Link to VoR: https://doi.org/10.31635/ccschem.025.202505638

These results were reproduced on the Cu/SiO_2 catalyst in methanol vapor, where the signals of $(CHO)Cu_1^*$ (m/z ratio of ~92 and 94), $(CH_2O)Cu_1^*$ (m/z of ~93 and 95), and $(CH_3O)Cu_1^*$ (m/z of ~94 and 96) were detected in the SVUV-PIMS, accompanied with the signals of methoxyl (m/z of 31) and formaldehyde (m/z of 30) species from methanol decomposition (m/z of 32, Figure 5b). In the equivalent tests, only methanol-related signals (Supporting Information Figure S32) were detected on the Cu/SiO_2-Me catalyst, with negligible signals associated with the $(CH_xO)Cu_1^*$ complex (Figure 5c). The results suggest that the methyl groups effectively minimize the $(CH_xO)Cu_1^*$ intermediates on the catalyst surface.

We performed density functional theory calculations to gain insights into the mechanism for minimizing the $(CH_xO)Cu_1^*$ intermediates on the Cu/SiO_2-Me. In the methanol-triggered Ostwald ripening of Cu nanoparticles by using a Cu_{13} cluster as a model, methanol initially reacted with the Cu surface to form multiple species. Among them, $*CHO$ and $*CH_3O$ were identified to be more stable on the Cu surface, which may have caused the detaching of Cu as a Cu_1 intermediate, but $*CO$ and $*CH_2O$ were prone to convert into CO and desorb from the Cu surface immediately (Supporting Information Figures S33 and S34). Following this insight, we compared the free energies of $(CHO)Cu_1^*$ and $(CH_3O)Cu_1^*$ intermediates from Cu nanocluster transportation on the silica surface with silanol (Si-OH) and methyl ($Si-CH_3$) groups. On the general SiO_2 surface, the $(CHO)Cu_1^*$ and $(CH_3O)Cu_1^*$ intermediates were activated on the Cu_{13} matrix, transported across the silanol groups, and finally docked onto an adjacent larger particle (Cu_{54} cluster as a model), with a free energy change of −0.91 eV (Figure 5d,f). This outcome indicates that the process is energetically favorable and aligns with the classical Ostwald ripening mechanism on the SiO_2.[33,35,42,47]

In contrast, for SiO_2-Me, the support surface had both silanol and methyl groups. Upon formation, the $(CH_3O)Cu_1^*$ and $(CHO)Cu_1^*$ species initially migrated onto the silanol group because of the interaction of silanol groups with them, proceeding with Gibbs free energy changes of 0.31 (Supporting Information Figure S35) and 0.13 eV (Supporting Information Figure S36), respectively. Due to the negligible interaction between the inert methyl groups with the Cu_1 intermedaites, the Cu_1 species could not migrate onto the methyl groups. Subsequent transportation of these species across the methyl groups encountered significantly higher energy barriers, amounting to 0.99 eV for $(CH_3O)Cu_1^*$ and 1.28 eV for $(CHO)Cu_1^*$ (Figure 5e). It should be noted that these Cu_1 intermediates are prone to be captured by the silanol nest on dealuminated zeolite, as shown in our previous work, which enables a redispersion of copper particles from larger to smaller ones.[28]

In contrast, the Gibbs free energy required for the migration of both intermediates exceeded 1.3 eV (Figure 5e), suggesting that the presence of methyl groups on the SiO_2 surface markedly elevated the energy barrier for the Cu_1-related intermediates during the surface transportation. In this case, the function of methyl groups worked for the Cu_1 intermediates, regardless of the size of the Cu cluster model used in this calculation. The hindered migration of Cu_1-related intermediates facilitated their rapid reattachment to the original Cu particles rather than abundant migration on the solid surface (Figure 5f), thereby preserving the stability against sintering. This observation was consistent with the SVUV-PIMS spectra, which gave negligible signals of Cu_1-related intermediates on the Cu/SiO_2-Me catalyst because the gas-phase intermediates were strongly related to the amount of intermediates on the solid surface, as controlled by their saturated vapor pressure.

In terms of the migration and coalescence pathway in the sintering behavior of Cu, we conducted a study on the migration of Cu nanoparticles on the SiO_2 and SiO_2-Me supports using steered molecular dynamics (SMD) simulations where a moving Hook's potential drives the horizontal movement of Cu_{55} cluster matrix along the reaction coordinate (Figure 5g,h and Supporting Information Figure S37). In these simulations, the subsequent coalescence processes were simulated using constrained molecular dynamics to allow for a more accurate depiction of its movement. Starting with the same position, the free energy barrier for Cu_{55} cluster migration on the SiO_2 was ~0.1 eV, which was lower than that on the SiO_2-Me support (~0.9 eV). In the Cu/SiO_2 system, the Cu cluster must surmount several energy barriers before reaching a neighboring Cu cluster with the highest free energy barrier of ~0.5 eV. Once the Cu clusters were coalesced, they became significantly exothermic, indicating that the Cu sintering was thermodynamically favorable. Conversely, the Cu cluster faced considerable difficulty in migrating across the methyl groups horizontally along the SiO_2 surface even driven by a moving Hook's potential. This finding aligns with the observed energy profile for the Cu/SiO_2-Me system (Figure 5h,i), which shows a rapid increase in free energy at the initial stage (①), followed by a plateau where the free energy remains constant (②), and a subsequent decrease in free energy at the final stage (③). Similar to that on the Cu/SiO_2, once the Cu cluster climbs over the methyl group, the coalescence of Cu clusters is also exothermic. We understand that the migration and coalescence of Cu nanoparticles under practical conditions are more intricate, and the model used here is smaller than the real-world catalysts. However, owing to the presence of methyl groups, both cluster migration and atom detachment from the Cu cluster hardly proceed, due to the significantly increased diffusion barrier for metal nanoparticles or atoms across the support surface.[15] This barrier helps stabilize the copper clusters, preventing them from sintering.

Citation: *CCS Chem.* **2025**, Just Published. DOI: 10.31635/ccschem.025.202505638
Link to VoR: https://doi.org/10.31635/ccschem.025.202505638

Conclusion

In summary, we have successfully stabilized Cu nanoparticles on a silica support modified with methyl groups, maintaining them against sintering under both harsh treatment and practical reaction conditions. Although the methyl groups have negligible interaction with the Cu species, they effectively hinder the migration of Cu nanoparticles and Cu_1-related intermediates across the silica surface, thereby significantly reducing the Cu sintering through both migration-coalescence and Ostwald ripening pathways. Consequently, we have realized a significant enhancement in durability for the catalytic hydrogenation of DMO to EG, even under ambient pressure conditions. This approach diverges from the conventional principle of stabilizing metal nanoparticles by constructing strong interaction regions on the support to immobilize them. Instead, our strategy increases migration barriers by constructing weak interaction regions, which can inform an efficient method to improve the stability of industrial catalyst for future applications. Furthermore, the methyl-functionalized Cu/SiO_2 catalyst may demonstrate broad applicability in other important reactions, including ester hydrogenation, CO_2 hydrogenation to methanol, and reverse water-gas shift.[49] However, for those reactions performed at high temperature and oxidative atmospheres, the decomposition of methyl groups may limit the application.

Supporting Information

Supporting Information is available and includes Figures S1–S37 and Tables S1–S2.

Conflict of Interest

There is no conflict of interest to report.

Funding Information

This work was supported by the National Key Research and Development Program of China (grant nos. 2022YFA1503502 and 2023YFA1507601), the National Natural Science Foundation of China (grant nos. 22288101, 22241801, and 22202176), the China Postdoctoral Science Foundation (CPSF) (grant no. 2024M752801), and the Postdoctoral Fellowship Program of CPSF (grant no. GZB20240650).

Acknowledgments

The authors appreciate Guoqing Zhu for her assistance in TEM characterization as well as the assistance of BL11B, the User Experiment Assist System, and the Chinese Academy of Sciences (CAS)-Shanghai Science Research Center of Shanghai Synchrotron Radiation Facility (SSRF). The authors are also grateful to be able to conduct SVUV-PIMS measurements using the Atomic & Molecular Physics Beamline (BL09U) at the National Synchrotron Radiation Laboratory in Hefei, China and for the Center for High-Performance Computing at Shanghai Jiao Tong University for providing the computing resources of the Siyuan-1 cluster.

References

1. Gates, B. C. Supported Metal Clusters: Synthesis, Structure, and Catalysis. *Chem. Rev.* **1995**, *95*, 511–522.
2. Campbell, C. T. The Energetics of Supported Metal Nanoparticles: Relationships to Sintering Rates and Catalytic Activity. *Acc. Chem. Res.* **2013**, *46*, 1712–1719.
3. Munnik, P.; de Jongh, P. E.; de Jong, K. P. Recent Developments in the Synthesis of Supported Catalysts. *Chem. Rev.* **2015**, *115*, 6687–6718.
4. Prieto, G.; Zečević, J.; Friedrich, H.; de Jong, K. P.; de Jongh, P. E. Towards Stable Catalysts by Controlling Collective Properties of Supported Metal Nanoparticles. *Nat. Mater.* **2013**, *12*, 34–39.
5. Mondelli, C.; Gözaydın, G.; Yan, N.; Pérez-Ramírez, J. Biomass Valorisation over Metal-Based Solid Catalysts from Nanoparticles to Single Atoms. *Chem. Soc. Rev.* **2020**, *49*, 3764–3782.
6. Kapil, N.; Weissenberger, T.; Cardinale, F.; Trogadas, P.; Nijhuis, T. A.; Nigra, M. M.; Coppens, M.-O. Precisely Engineered Supported Gold Clusters as a Stable Catalyst for Propylene Epoxidation. *Angew. Chem. Int. Ed.* **2021**, *60*, 18185–18193.
7. Hansen, T. W.; DeLaRiva, A. T.; Challa, S. R.; Datye, A. K. Sintering of Catalytic Nanoparticles: Particle Migration or Ostwald Ripening? *Acc. Chem. Res.* **2013**, *46*, 1720–1730.
8. Wynblatt, P.; Gjostein, N. A. Particle Growth in Model Supported Metal Catalysts—I. Theory. *Acta Metall.* **1976**, *24*, 1165–1174.
9. Parker, S. C.; Campbell, C. T. Kinetic Model for Sintering of Supported Metal Particles with Improved Size-Dependent Energetics and Applications to Au on TiO_2 (110). *Phys. Rev. B* **2007**, *75*, 035430.
10. Ouyang, R.; Liu, J.-X.; Li, W.-X. Atomistic Theory of Ostwald Ripening and Disintegration of Supported Metal Particles Under Reaction Conditions. *J. Am. Chem. Soc.* **2013**, *135*, 1760–1771.
11. Li, D.; Wang, Z.; Jin, S.; Zhu, M. Oxidation–Reduction Treatment Initiated in Situ Redispersion of the Supported Cu/Al_2O_3 Catalyst. *Chem Bio Eng.* **2024**, *1*, 541–547.
12. Wang, L.; Wang, L.; Meng, X.; Xiao, F.-S. New Strategies for the Preparation of Sinter-Resistant Metal-Nanoparticle-Based Catalysts. *Adv. Mater.* **2019**, *31*, 1901905.
13. Yin, P.; Hu, S.; Qian, K.; Wei, Z.; Zhang, L.-L.; Lin, Y.; Huang, W.; Xiong, H.; Li, W.-X.; Liang, H.-W. Quantification of Critical Particle Distance for Mitigating Catalyst Sintering. *Nat. Commun.* **2021**, *12*, 4865.

Citation: *CCS Chem.* **2025**, Just Published. DOI: 10.31635/ccschem.025.202505638
Link to VoR: https://doi.org/10.31635/ccschem.025.202505638

14. Zhan, W.; He, Q.; Liu, X.; Guo, Y.; Wang, Y.; Wang, L.; Guo, Y.; Borisevich, A. Y.; Zhang, J.; Lu, G.; Dai, S. A Sacrificial Coating Strategy Toward Enhancement of Metal–Support Interaction for Ultrastable Au Nanocatalysts. *J. Am. Chem. Soc.* **2016**, *138*, 16130–16139.
15. Hu, S.; Li, W.-X. Sabatier Principle of Metal-Support Interaction for Design of Ultrastable Metal Nanocatalysts. *Science* **2021**, *374*, 1360–1365.
16. Li, J.; Guan, Q.; Wu, H.; Liu, W.; Lin, Y.; Sun, Z.; Ye, X.; Zheng, X.; Pan, H.; Zhu, J.; Chen, S.; Zhang, W.; Wei, S.; Lu, J. Highly Active and Stable Metal Single-Atom Catalysts Achieved by Strong Electronic Metal–Support Interactions. *J. Am. Chem. Soc.* **2019**, *141*, 14515–14519.
17. Parastaev, A.; Muravev, V.; Huertas Osta, E.; van Hoof, A. J. F.; Kimpel, T. F.; Kosinov, N.; Hensen, E. J. M. Boosting CO_2 Hydrogenation via Size-Dependent Metal–Support Interactions in Cobalt/Ceria-Based Catalysts. *Nat. Catal.* **2020**, *3*, 526–533.
18. Tauster, S. J. Strong Metal-Support Interactions. *Acc. Chem. Res.* **1987**, *20*, 389–394.
19. van Deelen, T. W.; Hernández Mejía, C.; de Jong, K. P. Control of Metal-Support Interactions in Heterogeneous Catalysts to Enhance Activity and Selectivity. *Nat. Catal.* **2019**, *2*, 955–970.
20. Wang, T.; Hu, J.; Ouyang, R.; Wang, Y.; Huang, Y.; Hu, S.; Li, W.-X. Nature of Metal-Support Interaction for Metal Catalysts on Oxide Supports. *Science* **2024**, *386*, 915–920.
21. Li, X.; Pereira-Hernández, X. I.; Chen, Y.; Xu, J.; Zhao, J.; Pao, C.-W.; Fang, C.-Y.; Zeng, J.; Wang, Y.; Gates, B. C.; Liu, J. Functional CeO_x Nanoglues for Robust Atomically Dispersed Catalysts. *Nature* **2022**, *611*, 284–288.
22. Yao, D.; Wang, Y.; Li, Y.; Li, A.; Zhen, Z.; Lv, J.; Sun, F.; Yang, R.; Luo, J.; Jiang, Z.; Wang, Y.; Ma, X. Scalable Synthesis of Cu Clusters for Remarkable Selectivity Control of Intermediates in Consecutive Hydrogenation. *Nat. Commun.* **2023**, *14*, 1123.
23. Jones, J.; Xiong, H.; DeLaRiva, A. T.; Peterson, E. J.; Pham, H.; Challa, S. R.; Qi, G.; Oh, S.; Wiebenga, M. H.; Pereira Hernández, X. I.; Wang, Y.; Datye, A. K. Thermally Stable Single-Atom Platinum-on-Ceria Catalysts via Atom Trapping. *Science* **2016**, *353*, 150–154.
24. Farmer, J. A.; Campbell, C. T. Ceria Maintains Smaller Metal Catalyst Particles by Strong Metal-Support Bonding. *Science* **2010**, *329*, 933–936.
25. Zhou, W.; Thomas, J. M.; Shephard, D. S.; Johnson, B. F. G.; Ozkaya, D.; Maschmeyer, T.; Bell, R. G.; Ge, Q. Ordering of Ruthenium Cluster Carbonyls in Mesoporous Silica. *Science* **1998**, *280*, 705–708.
26. Wong, A.; Liu, Q.; Griffin, S.; Nicholls, A.; Regalbuto, J. R. Synthesis of Ultrasmall, Homogeneously Alloyed, Bimetallic Nanoparticles on Silica Supports. *Science* **2017**, *358*, 1427–1430.
27. Ciriminna, R.; Fidalgo, A.; Pandarus, V.; Béland, F.; Ilharco, L. M.; Pagliaro, M. The Sol–Gel Route to Advanced Silica-Based Materials and Recent Applications. *Chem. Rev.* **2013**, *113*, 6592–6620.
28. Liu, L.; Lu, J.; Yang, Y.; Ruettinger, W.; Gao, X.; Wang, M.; Lou, H.; Wang, Z.; Liu, Y.; Tao, X.; Li, L.; Wang, Y.; Li, H.; Zhou, H.; Wang, C.; Luo, Q.; Wu, H.; Zhang, K.; Ma, J.; Cao, X.; Wang, L.; Xiao, F.-S. Dealuminated Beta Zeolite Reverses Ostwald Ripening for Durable Copper Nanoparticle Catalysts. *Science* **2024**, *383*, 94–101.
29. Zheng, J.; Huang, L.; Cui, C.-H.; Chen, Z.-C.; Liu, X.-F.; Duan, X.; Cao, X.-Y.; Yang, T.-Z.; Zhu, H.; Shi, K.; Du, P.; Ying, S.-W.; Zhu, C.-F.; Yao, Y.-G.; Guo, G.-C.; Yuan, Y.; Xie, S.-Y.; Zheng, L.-S. Ambient-Pressure Synthesis of Ethylene GlycolCatalyzed by C_{60}-Buffered Cu/SiO_2. *Science* **2022**, *376*, 288–292.
30. Zheng, J.; Zhou, J.; Lin, H.; Duan, X.; Williams, C. T.; Yuan, Y. CO-Mediated Deactivation Mechanism of SiO_2-Supported Copper Catalysts During Dimethyl Oxalate Hydrogenation to Ethylene Glycol. *J. Phys. Chem. C* **2015**, *119*, 13758–13766.
31. Chen, C.-S.; Cheng, W.-H.; Lin, S.-S. Enhanced Activity and Stability of a Cu/SiO_2 Catalyst for the Reverse Water Gas Shift Reaction by an Iron Promoter. *Chem. Commun.* **2001**, (18), 1770–1771.
32. Gao, Z.; Ma, B.; Chen, S.; Tian, J.; Zhao, C. Converting Waste PET Plastics into Automobile Fuels and Antifreeze Components. *Nat. Commun.* **2022**, *13*, 3343.
33. van den Berg, R.; Parmentier, T. E.; Elkjær, C. F.; Gommes, C. J.; Sehested, J.; Helveg, S.; de Jongh, P. E.; de Jong, K. P. Support Functionalization to Retard Ostwald Ripening in Copper Methanol Synthesis Catalysts. *ACS Catal.* **2015**, *5*, 4439–4448.
34. Li, D.; Xu, F.; Tang, X.; Dai, S.; Pu, T.; Liu, X.; Tian, P.; Xuan, F.; Xu, Z.; Wachs, I. E.; Zhu, M. Induced Activation of the Commercial $Cu/ZnO/Al_2O_3$ Catalyst for the Steam Reforming of Methanol. *Nat. Catal.* **2022**, *5*, 99–108.
35. Lin, J.; Zhao, X.; Cui, Y.; Zhang, H.; Liao, D. Effect of Feedstock Solvent on the Stability of Cu/SiO_2 Catalyst for Vapor-Phase Hydrogenation of Dimethyl Oxalate to Ethylene Glycol. *Chem. Commun.* **2012**, *48*, 1177–1179.
36. Zhang, B.; Zhang, J.; Hua, M.; Wan, Q.; Su, Z.; Tan, X.; Liu, L.; Zhang, F.; Chen, G.; Tan, D.; Cheng, X.; Han, B.; Zheng, L.; Mo, G. Highly Electrocatalytic Ethylene Production from CO_2 on Nanodefective Cu Nanosheets. *J. Am. Chem. Soc.* **2020**, *142*, 13606–13613.
37. Zhang, Z.; Wang, Z.-L.; An, K.; Wang, J.; Zhang, S.; Song, P.; Bando, Y.; Yamauchi, Y.; Liu, Y. Ti^{3+} Tuning the Ratio of Cu^+/Cu^0 in the Ultrafine Cu Nanoparticles for Boosting the Hydrogenation Reaction. *Small* **2021**, *17*, 2008052.
38. Sun, Y.; Ma, Q.; Ge, Q.; Sun, J. Tunable Synthesis of Ethanol or Methyl Acetate via Dimethyl Oxalate Hydrogenation on Confined Iron Catalysts. *ACS Catal.* **2021**, *11*, 4908–4919.
39. Xu, C.; Chen, G.; Zhao, Y.; Liu, P.; Duan, X.; Gu, L.; Fu, G.; Yuan, Y.; Zheng, N. Interfacing with Silica Boosts the Catalysis of Copper. *Nat. Commun.* **2018**, *9*, 3367.
40. Sun, J.; Yu, J.; Ma, Q.; Meng, F.; Wei, X.; Sun, Y.; Tsubaki, N. Freezing Copper as a Noble Metal–Like Catalyst for Preliminary Hydrogenation. *Sci. Adv.* **2018**, *4*, eaau3275.
41. Zhao, S.; Yue, H.; Zhao, Y.; Wang, B.; Geng, Y.; Lv, J.; Wang, S.; Gong, J.; Ma, X. Chemoselective Synthesis of Ethanol via Hydrogenation of Dimethyl Oxalate on Cu/SiO_2:

Citation: *CCS Chem.* **2025**, Just Published. DOI: 10.31635/ccschem.025.202505638
Link to VoR: https://doi.org/10.31635/ccschem.025.202505638

Enhanced Stability with Boron Dopant. *J. Catal.* **2013**, *297*, 142–150.
42. Gong, J.; Yue, H.; Zhao, Y.; Zhao, S.; Zhao, L.; Lv, J.; Wang, S.; Ma, X. Synthesis of Ethanol via Syngas on Cu/SiO_2 Catalysts with Balanced Cu^0–Cu^+ Sites. *J. Am. Chem. Soc.* **2012**, *134*, 13922–13925.
43. Huo, J.; Tessonnier, J.-P.; Shanks, B. H. Improving Hydrothermal Stability of Supported Metal Catalysts for Biomass Conversions: A Review. *ACS Catal.* **2021**, *11*, 5248–5270.
44. Wang, H.; Gao, Z.; Sun, B.; Mu, S.; Dang, F.; Guo, X.; Ma, D.; Shi, C. Engineering Metal-Support Interaction to Construct Catalytic Interfaces and Redisperse Metal Nanoparticles. *Chem Catal.* **2023**, *3*, 100768.
45. Ihli, J.; Wong, W. C.; Noel, E. H.; Kim, Y.-Y.; Kulak, A. N.; Christenson, H. K.; Duer, M. J.; Meldrum, F. C. Dehydration and Crystallization of Amorphous Calcium Carbonate in Solution and in Air. *Nat. Commun.* **2014**, *5*, 3169.
46. Xu, Y.; Li, X.; Gao, J.; Wang, J.; Ma, G.; Wen, X.; Yang, Y.; Li, Y.; Ding, M. A Hydrophobic FeMn@Si Catalyst Increases Olefins from Syngas by Suppressing C1 By-Products. *Science* **2021**, *371*, 610–613.
47. Wang, M.; Yao, D.; Li, A.; Yang, Y.; Lv, J.; Huang, S.; Wang, Y.; Ma, X. Enhanced Selectivity and Stability of Cu/SiO_2 Catalysts for Dimethyl Oxalate Hydrogenation to Ethylene Glycol by Using Silane Coupling Agents for Surface Modification. *Ind. Eng. Chem. Res.* **2020**, *59*, 9414–9422.
48. Ye, R.-P.; Lin, L.; Wang, L.-C.; Ding, D.; Zhou, Z.; Pan, P.; Xu, Z.; Liu, J.; Adidharma, H.; Radosz, M.; Fan, M.; Yao, Y.-G. Perspectives on the Active Sites and Catalyst Design for the Hydrogenation of Dimethyl Oxalate. *ACS Catal.* **2020**, *10*, 4465–4490.
49. Gawande, M. B.; Goswami, A.; Felpin, F.-X.; Asefa, T.; Huang, X.; Silva, R.; Zou, X.; Zboril, R.; Varma, R. S. Cu and Cu-Based Nanoparticles: Synthesis and Applications in Catalysis. *Chem. Rev.* **2016**, *116*, 3722–3811.

Citation: *CCS Chem.* **2025**, Just Published. DOI: 10.31635/ccschem.025.202505638
Link to VoR: https://doi.org/10.31635/ccschem.025.202505638